Noname manuscript No.
(will be inserted by the editor)

A Hyper Elasticity Method for Interactive Virtual Design of Hearing Aids

A Parallel Method for general Non-linear Hyper Elasticity Modelling

Sune Darkner · Kenny Erleben

Received: date / Accepted: date

Abstract We present a computational efficient method for isotropic hyper elasticity based on functional analysis. By selecting a class of shape functions, we arrive at a computational scheme which yields very sparse tensors. This enables fast computations of the hyper elastic energy potential and its derivatives. We achieve efficiency and performance through the use of shape functions that are linear in their parameters and through rotation into the eigen space of the right Cauchy-Green strain tensor. This makes near real time evaluation of hyper elasticity of complex meshes on CPU relatively easy to implement. The approach does not rely on a specific shape function or material model but offers a general framework for isotropic hyper elasticity. The method is aimed at interactive and accurate non-linear hyper elastic modeling for a wide range of industrial virtual design applications, which we exemplify by insertion of hearing aid domes into the ear canal. We validate the method for tetrahedral meshes with linear shape functions with an Ogden material model by comparing simulations to deformations of real material. We illustrate the use of other shape functions and models using uniform cubic B-splines in combination with Riemanian elasticity.

Keywords Hyper elasticity · Interactive Design · Virtual Prototyping · General Framework

Sune Darkner and Kenny Erleben
Univrsity of Copenhagen, Dpt. of computer Science
Tel.: +45 26129987
E-mail: {darkner,erleben}@diku.dk *Present address:* Universitetesparken 1 DK-2100 Copenhagen, Denmark

1 Need for Accuracy and Large Deformation Handling in Interactive Simulations

In production companies, there is a need for rapid development tools and test of proof-of-concepts as fast as possible and preferably interactive in which accuracy is of crucial importance. Traditional computer graphics methods for interactive simulation of deformable models, though fast, cannot be applied to industrial virtual design. These methods cannot handle large deformation while simulating materials accurately enough. When modeling mechanical solids the hyper elastic model is most often used in the context of Finite Element Modeling. Elasticity is in general rather complex to estimate, especially due to its highly non-linear structure [6]. As a result, numerous approximations have been suggested such as linear elasticity and co-rotational formulation. However, due to the fact that these are approximations and the elasticity is highly non-linear, such models are only good for small deformations. In practice these only model realistic deformations so small that they cannot be seen by the naked eye. Thus, an efficient scalable and parallel method for calculation of the hyper elasticity is needed especially in interactive computer simulations. As an example and motivating case for this need of more correct models and methods, Figure 1 illustrates a prototype design optimization tool. Here, the task is shape optimization with respect to correct insertion of hearing domes into the ear canal. The general task is to investigate the fit of the dome in a particular ear, enabling further calculations. The tool is intended for visual inspection of new design ideas.

We present a parallel and fast computational method for the quasi-static equilibrium simulation of isotropic hyper elastic materials. Our method is based on functional formulation, as opposed to variational, shape func-

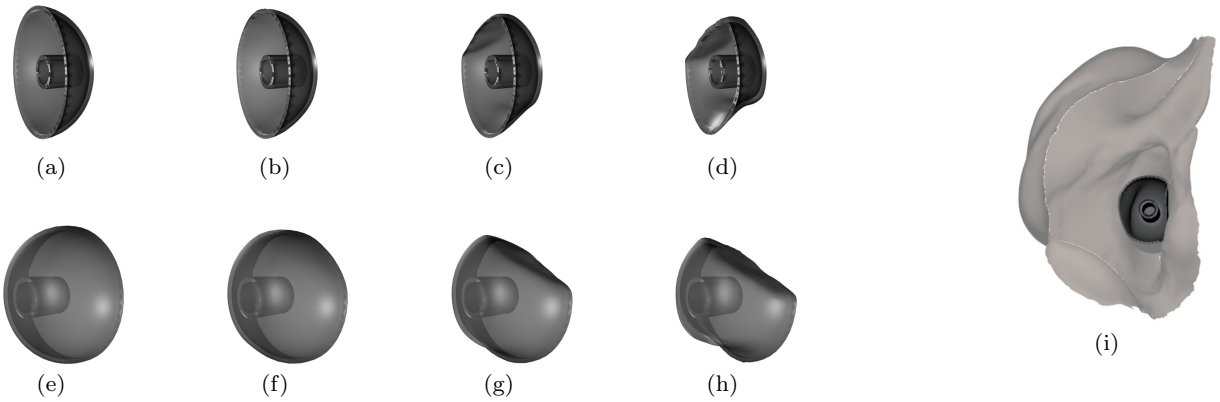

Fig. 1 Virtual design tools for optimizing hearing aid production requires both fast performance as well as accurate simulations of large deformations and nonlinear materials. In (a)-(d) we have shown frames from an animation of a dome fitting simulation. In (e)-(h) the same animation is shown form a different view. In (i) the dome is shown inside the ear canal.

tions which are linear in their parameters and decomposition into principal stretches. From this, we arrive at a formulation where the tensors become very sparse thus making fast efficient and accurate calculations possible. Furthermore, we can easily rotate into the eigen space of the right Cauchy-Green strain tensor making the implementation of a wide range of hyper elastic models very easy through the use of the chain rule. The method exploits analytical derivatives for the strain energy density functions by insertion of the generalized shape functions and the use of the chain rule. We describe the math behind a fast implementation scheme of isotropic hyper elastic materials. The scheme supports a wide range of material models such as the St. Venant–Kirchoff, Riemannian [27] elastic material model, the Ogden [26] material model or models such as volume preservation. We assume global differentiability; however, we show that local linear shape functions numerically are stable as well. The framework originates in geometry and is based on the right Cauchy-Green strain tensor and its eigen values (squared principal stretches). We form analytical derivatives of the eigen values with respect to the transformation parameters independent of the parameterization.

The rest of the paper is organized in the following way: Section 2 present the related work, Section 3 presents the general approach, Section 4 presents the experiments and validation as well as flexibility of the method. Finally we summarize in Section 5 and present our conclusion in Section 6.

2 Related Work on Interactive Physical Accurate Deformable Models

Deformable models cover a wide range of simulations from solids, shells, rods, wires to cloth and hair [2,5,8, 15,29]. The methods range from physical based to more ad hoc or geometry inspired methods [7,9,23]. We need to handle real materials undergoing large deformations in an interactive application. Thus, we focus only on work relevant to interactive physical based simulation of solids. Other interactive works are not well suited for accurate material simulation such as the versatile method and position-based-physics [22,35].

Initial work on deformable models were based on finite difference methods and differential geometry measures such as first and second fundamental forms [34]. Green strain and Piola Kirkhoff stress tensors are often applied for offline animation methods [3,4,11,16,25,32, 33]. Whereas the co-rotational linear FEM – based on Cauchy strain and stress tensors – is often favored for interactive animation [12,13,20,21,36,38]. It is mostly FEM methods that have been used and are in our view considered the dominating methods. There are few examples of finite volume methods as well [32]. An alternative paradigm is mesh free methods similar to SPH [24]. Overall, one can characterize this work as using linear shape functions for interpolation. Our approach only considers minimization of the strain energy and as such we have no explicit need to work with strain and stress tensors. However, we do form the right Cauchy–Green strain tensor since our material models is expressed in terms of its invariants. These invariants are strongly related to polar decomposition of the deformation gradient, particular useful in computer graphics for dealing with inversion of elements [14, 17, 28]. Several methods have been used for this singular value

decomposition, polar decomposition, linear regression by energy minimization in a quaternion representation. We disregard inversion, though handle it numerically, as this is not an issue for real world materials, and exploit the found eigen values to make a favorable material representation. Tetrahedral meshes using four node elements (T4) are by far the most used meshes for FEM methods in computer graphics. However, there are examples of other mesh types such as hexahedral meshes [18]. In this work, we show examples using T4 meshes. However, our theory generalizes to other types of elements which we exemplify with uniform cubic B-splines. The most widely used material models in computer graphics are the neo-Hookean and St. Venant–Kirkhoff material models. These can also be included in our work as well as Ogden material model, Riemanian elasticity and a volume preservation strain energy model. In combination, these choices in an easy to implement method that is massively parallelizable and very robust towards large deformations. Further, it offers a generic framework for interchanging material models and shape functions for the elements.

3 Static Equilibrium Method for Hyper Elastic Materials

When inserting a dome into the ear canal, we seek to minimize the strain energy subject to the constraint that the dome does not interpenetrate the tissue. The strain energy density function ψ can be tailored specifically for the type of material and behavior desired. In this work, we have looked at four different functions, volume preservation, Riemanian elasticity, St. Venant–Kirchhoff and Ogden material models. All models that can be formulated in terms of the principal stretches (see below).

The deformation is given by $\mathbf{x} = \phi(\mathbf{X})$ where $\mathbf{X}, \mathbf{x} \in \mathbb{R}^3$ is the material and spatial coordinates respectively. The elastic strain energy is given by the material energy functional

$$W = \int_V \psi\left(\mathbf{F}(\mathbf{X}), \mathbf{X}\right) dV \tag{1}$$

where the deformation gradient is given by

$$\mathbf{F} = \frac{\partial \phi(\mathbf{X})}{\partial \mathbf{X}} = \nabla_0 \mathbf{x} \tag{2}$$

Here $\mathbf{x} = \phi(\mathbf{X})$ is the material to spatial deformation. We seek the unknown deformation function $\phi : \mathbf{X} \mapsto \mathbf{x}$ such that the variation of the strain energy vanishes. That is; we wish to find the function ϕ that fulfills the Euler–Lagrange equations,

$$\frac{\partial \psi}{\partial \phi} - \sum_{i=1}^{3} \frac{\partial}{\partial X_i}\left(\frac{\partial \psi}{\partial \mathbf{F}_{i*}}\right) = 0, \tag{3}$$

For isotropic hyper elastic materials the strain energy density function is independent of the spatial coordinates, thus $\frac{\partial \psi}{\partial \phi} = 0$. Using the Euler-Lagrange equation, our problem can be written compactly as [1]

$$\nabla_0 \cdot \frac{\partial \psi}{\partial \mathbf{F}} = \mathbf{0} \tag{4}$$

To avoid solving for an arbitrary unknown function ϕ, we choose an approximation having the form

$$\phi(\mathbf{X}) \approx \hat{\phi}(\mathbf{X}) = \mathbf{X} + \sum_j B_j(\mathbf{X}) \hat{\mathbf{u}}_j \tag{5}$$

where all $B_j(\mathbf{X})$'s are shape/weight functions and $\hat{\mathbf{u}}_j$ can be interpreted either as some discrete nodal displacements or as a parameter vector for the shift of basis given by $B_j(\mathbf{X})$. This approximation brings a finite-element method flavor to our solution method. Our approximation gives us

$$\mathbf{F} \approx \hat{\mathbf{F}} = \nabla_0 \left(\mathbf{X} + \sum_j B_j(\mathbf{X}) \hat{\mathbf{u}}_j\right) \tag{6a}$$

$$= \mathbf{I} + \sum_j \nabla_0 \left(B_j(\mathbf{X}) \hat{\mathbf{u}}_j\right) \tag{6b}$$

$$= \mathbf{I} + \sum_j \hat{\mathbf{u}}_j \otimes \nabla_0 B_j(\mathbf{X}) \tag{6c}$$

Next we substitute the approximation into our strain energy functional to obtain a function

$$\hat{W} = \int_V \psi\left(\hat{\mathbf{F}}(\mathbf{X}), \mathbf{X}\right) dV \tag{7a}$$

$$= \int_V \psi\left(\left(\mathbf{I} + \sum_j \hat{\mathbf{u}}_j \otimes \nabla_0 B_j(\mathbf{X})\right), \mathbf{X}\right) dV \tag{7b}$$

The consequence is that rather than solving the variational problem given by the functional W, we can minimize the function $\hat{W}$ with respect to the unknown $\hat{\mathbf{u}}_j$ values. That is; we solve for the first order optimizer given by the zero gradient[2]

$$\frac{\partial \hat{W}}{\partial \hat{\mathbf{u}}_j} = \int_V \frac{\partial \psi}{\partial \mathbf{F}} : \frac{\partial \hat{\mathbf{F}}}{\partial \hat{\mathbf{u}}_j} dV = 0 \quad \forall j \tag{9}$$

[1] Observe that this is in fact the Cauchy equation for the case with no body or inertia forces

[2] The result of the chain rule can be written in a more convenient form using the contraction as we have

$$\frac{\partial \psi}{\partial \mathbf{F}} : \frac{\partial \hat{\mathbf{F}}}{\partial \hat{\mathbf{u}}_j} = \sum_a \sum_b \frac{\partial \psi}{\partial \mathbf{F}_{ab}} \frac{\partial \hat{\mathbf{F}}_{ab}}{\partial \hat{\mathbf{u}}_j} \tag{8}$$

Observe that the term $\frac{\partial \psi}{\partial \mathbf{F}}$ is in fact the first Piola–Kirchhoff stress tensor. We postpone giving a final formula for the term $\frac{\partial \hat{\mathbf{F}}}{\partial \hat{\mathbf{u}}_j}$. Instead, we will here describe how (9) is solved. We opt for simplicity, robustness and ease of implementation and apply an iterative approach using a gradient descent method

$$\hat{\mathbf{u}}^{k+1} = \hat{\mathbf{u}}^k - \tau^k \frac{\partial \hat{W}}{\partial \hat{\mathbf{u}}_j} \quad \forall j \tag{10}$$

where τ^k is the step length of the k^{th} iteration resulting in a damped line–search to globalize our method and prevent overshooting. Observe that the minimization problem could be solved using other types of numerical methods. For instance, we have experience using the L-BFGS method [37]. This is a quasi Newton method which only needs to evaluate the strain energy gradient in each approximation.

We solve the integral given in (9) using some numerical integration method such as the midpoint rule or similar. We continue the iteration (10) until the norm of the strain gradient is sufficiently small or the change in the deformation $\mathbf{F}$ is insignificant. In our implementation we use a threshold value of 10^{-7} for both of these stopping criteria.

3.1 Penetration Constraints

To deal with penetrations, we use a soft constrain approach. We employ a scalar field based on an Euclidian distance transform [1, 19, 31] which acts as a soft constraint based on the geometry. This is the simplest way when simulating with an impression of the ear. This can be viewed as a surface registration problem as in [10].

$$\mathcal{F}[S_1, S_2, \boldsymbol{\phi}] = \int_{S_2 \cap \boldsymbol{\phi} \circ S_1} \mathcal{D}[S_2, \boldsymbol{\phi} \circ S_1] ds \tag{11}$$

where $\mathcal{D}$ is the penalty function, S_1 and S_2 are the interacting surfaces

For the material verification, we use a hard constraint where we lock the position of the top and bottom of the object increasingly applying the displacement to the top of the cylinder to maintain our diffeomorphism avoiding mesh inversions.

3.2 Real World Materials

The physical behavior of an isotropic hyper elastic material is invariant with respect to translation, rotation and the path taken. Therefore we can formulate any isotropic strain energy density function as a function of the eigen values λ_i^2 for $i = 1, 2, 3$ of the right Cauchy-Green strain tensor

$$\mathbf{C} = \mathbf{F}^T \mathbf{F} = \sum_i \lambda_i^2 \mathbf{N}_i \otimes \mathbf{N}_i \tag{12}$$

where $\mathbf{N}_i$ are the respective eigenvectors[3]. Among strain energy density functions we have used are volume preservation, Riemanian [27], St. Venant–Kirchoff, and Ogden [26]. These functions are given as

$$\psi_{\text{vol}} = (\prod_i \lambda_i^{\frac{1}{2}} - 1)^2, \tag{13a}$$

$$\psi_{\text{rie}} = \frac{\mu}{4} \sum_i \log^2 \lambda_i + \frac{\lambda}{8} \left(\sum_i \log \lambda_i \right)^2, \tag{13b}$$

$$\psi_{\text{svk}} = \frac{\mu}{4} \sum_i (\lambda_i^{\frac{1}{2}} - 1)^2 + \frac{\lambda}{8} \left(\sum_i (\lambda_i^{\frac{1}{2}} - 1) \right)^2 \tag{13c}$$

$$\psi_{\text{ogden}} = \sum_{p=1}^{N} \frac{\mu_p}{\alpha_p} \left(\lambda_1^{\frac{\alpha_p}{2}} + \lambda_2^{\frac{\alpha_p}{2}} + \lambda_3^{\frac{\alpha_p}{2}} - 3 \right) \tag{13d}$$

where μ and λ are the Lame constants. Observe that the first Piola–Kirchhoff stress tensor may be written as a transformation of the second Piola–Kirchhoff stress tensor $\mathbf{S}$

$$\frac{\partial \psi}{\partial \mathbf{F}} = \mathbf{P} = \mathbf{FS} \tag{14}$$

The second Piola–Kirchhoff stress tensor may be found through the relation

$$\mathbf{S} = 2 \sum_i \frac{\partial \psi}{\partial \lambda_i^2} (\mathbf{N}_i \otimes \mathbf{N}_i) \tag{15}$$

Combining this with (9) we now have

$$\frac{\partial \psi}{\partial \mathbf{F}} : \frac{\partial \hat{\mathbf{F}}}{\partial \hat{\mathbf{u}}_j} = 2\mathbf{F} \left(\sum_i \frac{\partial \psi}{\partial \lambda_i^2} (\mathbf{N}_i \otimes \mathbf{N}_i) \right) : \frac{\partial \hat{\mathbf{F}}}{\partial \hat{\mathbf{u}}_j} \tag{16}$$

It is straight forward to compute $\frac{\partial \psi(\phi)}{\partial \lambda_i^2}$ i.e. for Ogden material model

$$\frac{\partial \psi_{\text{ogden}}(\phi)}{\partial \lambda_i^2} = \sum_{p=1}^{N} \mu \lambda_i^{\frac{\alpha}{2} - 1} \tag{17}$$

Now from (6) we find that

$$\frac{\partial \hat{\mathbf{F}}}{\partial \hat{\mathbf{u}}_j} = \frac{\partial \sum_j \hat{\mathbf{u}}_j \otimes \nabla_0 B_j}{\partial \hat{\mathbf{u}}_j} \tag{18}$$

which can be calculated as

$$\frac{\partial \hat{\mathbf{F}_{ab}}}{\partial (u_j)_c} = \begin{cases} (\nabla_0 B_j)_c & \text{iff a=c} \\ 0 & otherwise \end{cases} \tag{19}$$

[3] One may also use the eigen values of the left Cauchy–Green strain tensor $\mathbf{b} = \mathbf{F}\mathbf{F}^T$ as they are the same.

3.3 Computational Mesh and Basis Function

Given the parameterization in (5) we are restricted to select shape function which meet the criteria of differentiability everywhere and are of the form given by (5). This will ensure a conforming function over the entire domain. We will briefly discuss two different choices of shape functions that we have successfully applied. One is based on a tetrahedral mesh using linear interpolation on the tetrahedral elements and the other interpolation is based on a regular grid using cubic B-splines. The linear interpolation is not conforming at the interface between elements. However, it is everywhere else and we choose to neglect this inconsistency and show that this in practice works fine. The cubic uniform B-splines on the other hand are conforming. However, implementation of hard constraints is quite difficult as these can only be found iteratively. One way of using the B-splines is to embed the tetrahedral mesh in the regular B-spline grid and work with soft constraints on penetrations.

4 Results and Experiments

We have aimed at verifying our method by examining various properties in isolation. We use tetrahedral meshes and the Ogden material model for the experiment if not otherwise stated. In particular, mesh convergence and volume preservation are treated. We evaluate performance and convergence properties, validating the physical correctness by studying accuracy in comparison to a real world material. We discuss the hearing aid application and we exemplify the use of B-splines and Riemanian elasticity.

Implementation: The reference implementation of the method presented has been implemented in C++ using multi-threading and interfacing to MATLAB. The optimizer used is an off-the-shelf version of L-BFGS unless otherwise stated. The optimizer is not optimized particularly for the problem at hand.

Mesh Convergence: Our hypothesis is that the simulation result will globally converge when the overall mesh element size is reduced. In this experiment we create a cylinder mesh of uniform regular size and use average tetrahedra volume as an indicator for the average element size. We simulate a simple cylinder of homogenous material squeezed to a certain degree. The simulation is repeated with reduced average volume (roughly a factor of 8) until the simulation result is no longer changing (within sufficient precision). This gives us 4 meshes with 430000, 55200, 6600 and 750 elements. The resulting meshes have full point correspondence from the low resolution mesh to the high resolution mesh. As a measure of convergence we compute the average distance and standard deviation between corresponding points. As the model is polynomial and the basis is linear, we expect the convergence to be proportional to $\frac{1}{x}$, where x is the average edge length or the cubic root of the average element volume. Figure 2 shows our results.

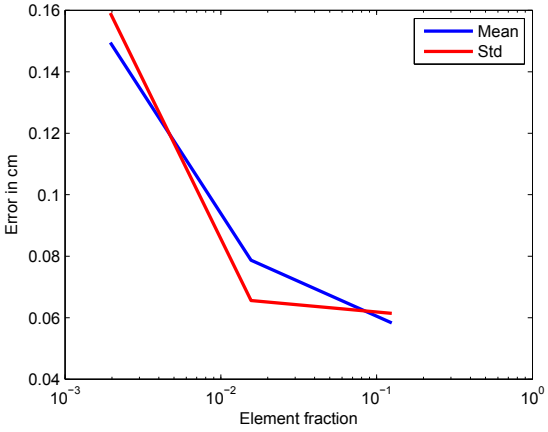

Fig. 2 The reference mesh has 430000 elements. The error should behave as $\frac{1}{x}$, where x is the edge length. The experiments confirm this. Notice that it is sufficient to use 6600 elements to achieve relative low error. Furthermore we see that even 750 elements perform quite well.

Volume Preservation: Our hypothesis is that the simulation will preserve volume more when the number of solver iterations is increased. In this experiment we create a cylinder mesh of uniform regular size and of homogenous material. We subject the cylinder to constraint faking a squeeze between two planar plates. We perform only a single simulation step in each simulation run. For the single simulation step, we vary the number of solver iterations used. We plot the max, min and average volume fraction of each element ($\frac{Vol_{deformed}}{Vol_{nondeformed}}$) which is equivalent to the determinant of the deformation gradient as a function of solver iterations. The average volume is fully restored after 60 iterations. Figure 3 shows our results.

Computing Time: Hyper elasticity comes at a price. The proposed method can to some extend remedy this. We are satisfied with 40-50 iterations per second, which will be supported with up to roughly 7000 tetrahedra. To illustrate the computing time, we simulate an elastic block of homogenous material squeezed between two rigid flat plates. The wall-clock time of the overall simulation is measured and plotted log-log as a function of the number of elements used in the block mesh. The mesh is generated to have regular uniform elements and each simulation is run until an absolute tolerance is reached. As can be seen from the volume plot, we have decent accuracy after 40 iterations. As

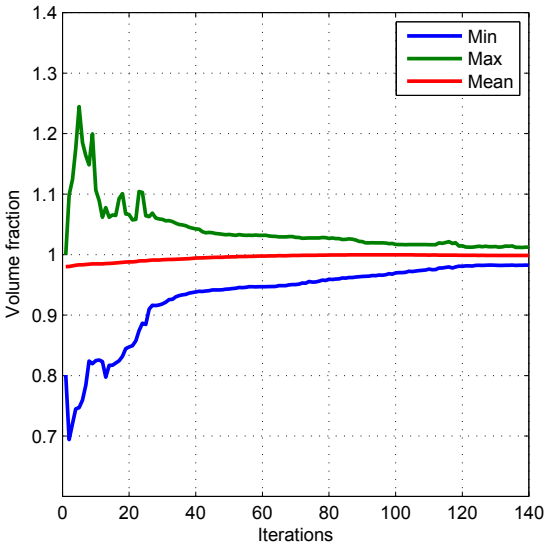

Fig. 3 Volume preservation, notice that as the solver iterations are increased, the volume preservation is improved. In particular, after 40 iterations the volume is suitably preserved for our purpose.

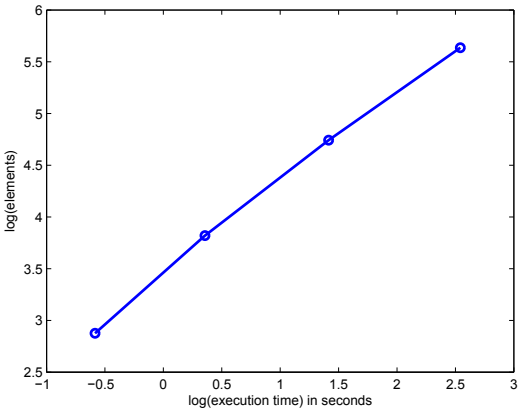

Fig. 4 The evaluation time as function of the number of elements in a log/log plot. This figure shows linear dependence between the number of elements and evaluation time.

this is an interactive design evaluation tool, we expect the user to move the object into place. We are satisfied performance yielding 1 second latency from placement to satisfying result. It is a well known fact that human response time is on average 0.5 seconds. Thus 1 second is sufficiently fast to provide interactive evaluation. Figure 4 shows our results.

Convergence Rate: We have used 3 different optimization routines: Gradient descent, L-BFGS and a Newton method with estimated 2nd order structure. As the Newton method converges in 4 iterations we have left it out of the convergence plot in Figure 5. We have chosen a mesh element size that gives us good results.

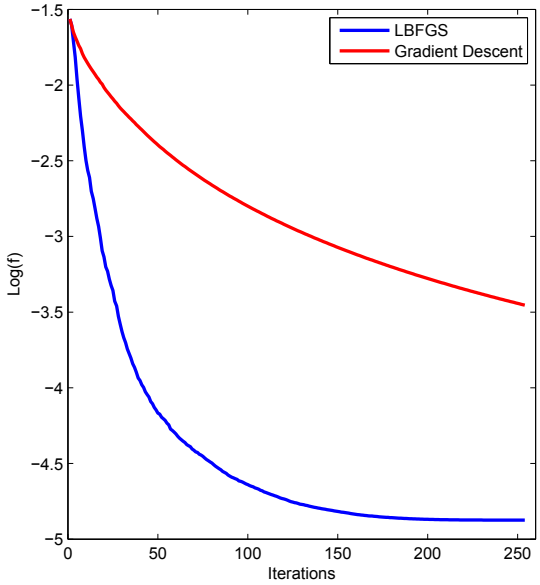

Fig. 5 Super linear convergence is obtained in the first 5 iteration with L-BFGS. Gradient descent is linear. Notice that after 254 iterations we reach machine precision.

We make a log plot of the residual error of the solver as a function of solver iterations. We expect gradient descent to have linear convergence, L-BFGS to have super linear and Newton to be quadratic. The plot shows that L-BFGS only has super linear convergence in the first 5 iterations and then linear, gradient descent has sub linear convergence. As seen in Figure 5 L-BFGS converges much faster than gradient descent. The Newton method behaves as expected and reaches it optima in 4 iterations, i.e quadratic. From the number of FLOPS and parameters we expect the strain energy density function to have a precision of 10^{-7} which has been confirmed experimentally. Figure 5 shows our results.

Accuracy: Our hypothesis is that our method is capable of accurately simulating the deformation behavior of isotropic nonlinear rubberlike materials used for manufacturing domes in hearing aids. To validate this we compare our simulation results against real-world material deformations. We have created cylindrical blocks of homogenous materials (silicone) 30 mm high and 40mm in diameter, which we fix between two metal brackets. Figure 7 shows our experimental setup. By adjusting 3 bolts we are able to accurately (within 0.2 mm) adjust the amount of compression of the material which we then photograph. For each real-world experiment we conduct a similar simulated experiment and from the simulation results we project a silhouette onto a plane. Next we make a comparison of the shape of the simulated silhouette against the real-world sil-

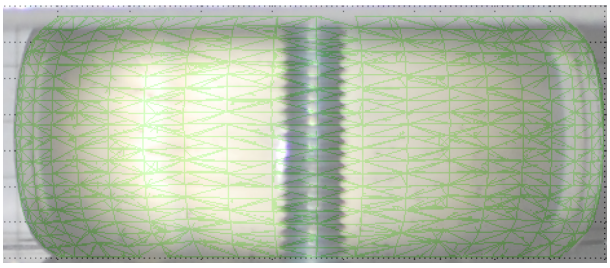

Fig. 6 Our real world experiment used to obtain true deformation shapes of materials overlaid with a simulation of a similar rubber-like cylinder. As seen the difference is almost non-existing.

(a) (b) (c)

Fig. 7 The experimental setup to capture the hyper elastic deformation under known displacement. In (a) the deformation rig, (b) the setup (c) the undeformed cylinder of silicone.

houette by using the DICE-measure.

$$\mathbf{D}(r, s) = 0.996$$

Here r is the real-world silhouette and s the simulated one. We expect our method to accurately capture the deformation of the rubber material, and as can be seen in figure 6, this is very accurate.

Application to hearing aid dome: With this knowledge about the behavior of the model we have applied it to the simulation of insertion of a dome into the human ear canal. The dome consists of 20274 elements and 6062 nodes. The mesh was generated using tetgen [30]. Thus, it has very varying element size and some with very small dihedral angles limiting the step size, thus increasing the required number of iterations. The dome has been fitted using a soft constraint to squeeze it into the ear canal as described above and the core cylinder has been limited to translation only perpendicular to the ear canal wall. The core cannot deform in the real world as it is filled with a speaker transmitting the sound into the ear. The result of a simulation at a given position can be seen in Figure 1(i).

Cubic B-splines: Finally, we have made similar experiments using B-splines. The use of B-splines offers flexibility to the model and enables easy deployment of multi-grid methods. In this simulation we have substituted the Ogden material model with Riemanian elasticity (13) to demonstrate interchangeability between models. We have simulated a cube on a planar surface

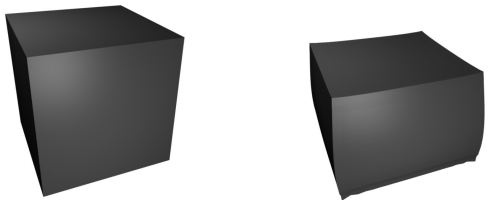

(a) (b)

Fig. 8 Our simulation using cubic B-splines.(a) the undeformed cube (b) the deformed cube under gravity.

with fixed base in a constant gravity field. As can be seen, the model allows for compressibility. This particular model has 48000 tetrahedra, but is evaluated using a $10 \times 10 \times 10$ B-spline grid with roughly 68000 evaluation points. Figure 8 shows the result.

4.1 Discussion of Experiments

The experiments are designed to validate the method and show that it indeed is a good method for isotropic hyper elastic materials. As our simulation experiments are conducted in a perfect world, factors like sliding of the material on the metal brackets, small inhomogeneities, fractures, compressibility and thermal constants etc. are not included. Furthermore, the comparison with real-world experiments suffers from lens distortion and non-calibrated camera, though neglectable still present. However, we are convinced that the experimental setup is sufficient to validate the deformation and the results are very convincing.

5 Discussion

The method described in this paper can be implemented in parallel and offers an easy way of switching between different kinds of isotropic elasticity models. The performance is to some extend dependent on the parameterization $\boldsymbol{\phi}$, e.g. a B-spline in 3D will have 192 parameters where as the tetrahedral only has 12 from which the strain tensor is computed. Thus, one should when solving a specific problem, carefully select the appropriate parameterization such that speed, accuracy and performance fits the given task.

Future work will include extension of the model to non-isotropic and plastic materials. In addition, there is room for improvement with respect to the solver which can be tailored specifically to the method.

6 Summary and Conclusion

We have presented an efficient and accurate method for implementing hyper elastic models based on functional analysis. Using the chain rule and rotation into eigen space of the right Cauchy-Green strain tensor, we show how sparsity of the tensor is obtained. The method is illustrated using Ogden and Riemanian as well as both uniform cubic B-splines and linear shape functions on tetrahedral meshes. This illustrates the generality of the method with respect to shape functions and models. We have verified that the method models isotropic hyper elastic material sufficiently accurately, to such a degree that it can be used in an industry setting. We verified the numerical properties of the method, the scaling with number of elements or integration points and have shown that it is accurate down to 10^{-7}. From our experiments, we can observe that the performance of the current implementation is sufficient for an interactive virtual design validation tool. The method has been applied to insertion of a hearing aid dome into a ear with success.

Acknowledgements This work is supported by the Oticon foundation

References

1. Baerentzen, J.A., Aanaes, H.: Signed distance computation using the angle weighted pseudonormal. IEEE Transactions on Visualization and Computer Graphics **11**, 243–253 (2005)
2. Baraff, D., Witkin, A.: Large steps in cloth simulation. In: SIGGRAPH '98: Proceedings of the 25th annual conference on Computer graphics and interactive techniques, pp. 43–54. ACM, New York, NY, USA (1998)
3. Barbič, J., James, D.L.: Real-time subspace integration for st. venant-kirchhoff deformable models. ACM Trans. Graph. **24**, 982–990 (2005)
4. Bargteil, A.W., Wojtan, C., Hodgins, J.K., Turk, G.: A finite element method for animating large viscoplastic flow. ACM Trans. Graph. **26** (2007)
5. Bergou, M., Wardetzky, M., Robinson, S., Audoly, B., Grinspun, E.: Discrete elastic rods. ACM Trans. Graph. **27**(3), 1–12 (2008)
6. Bonet, J., Wood, R.D.: Nonlinear continuum mechanics for finite element analysis. Cambridge University Press (2008)
7. Botsch, M., Pauly, M., Gross, M., Kobbelt, L.: Primo: coupled prisms for intuitive surface modeling. In: Proceedings of the fourth Eurographics symposium on Geometry processing, SGP '06, pp. 11–20. Eurographics Association, Aire-la-Ville, Switzerland, Switzerland (2006)
8. Bridson, R., Fedkiw, R., Anderson, J.: Robust treatment of collisions, contact and friction for cloth animation. In: SIGGRAPH '02: Proceedings of the 29th annual conference on Computer graphics and interactive techniques, pp. 594–603. ACM, New York, NY, USA (2002)
9. Choi, M.G., Ko, H.S.: Modal warping: Real-time simulation of large rotational deformation and manipulation. IEEE Transactions on Visualization and Computer Graphics **11**, 91–101 (2005)
10. Darkner, S., Vester-Christensen, M., Larsen, R., Paulsen, R.R., Nielsen, C.: Automated 3D rigid registration of open 2D manifolds. In: Proc. From Statistical Atlases to Personalized Models Workshop, MICCAI 2006, pp. 19–22
11. Debunne, G., Desbrun, M., Cani, M.P., Barr, A.H.: Dynamic real-time deformations using space & time adaptive sampling. In: Proceedings of the 28th annual conference on Computer graphics and interactive techniques, SIGGRAPH '01, pp. 31–36. ACM, New York, NY, USA (2001)
12. Galoppo, N., Otaduy, M., Tekin, S., Gross, M., Lin, M.: Soft articulated characters with fast contact handling. Computer Graphics Forum **26**(3), 243–253 (2007)
13. Galoppo, N., Otaduy, M.A., Moss, W., Sewall, J., Curtis, S., Lin, M.C.: Controlling deformable material with dynamic morph targets. In: Proceedings of the 2009 symposium on Interactive 3D graphics and games, I3D '09, pp. 39–47. ACM, New York, NY, USA (2009)
14. Georgii, J., Westermann, R.: Corotated finite elements made fast and stable. In: Proceedings of the 5th Workshop On Virtual Reality Interaction and Physical Simulation, pp. 11–19 (2008)
15. Grinspun, E.: A discrete model of thin shells. In: SIGGRAPH '06: ACM SIGGRAPH 2006 Courses, pp. 14–19. ACM, New York, NY, USA (2006)
16. Irving, G., Schroeder, C., Fedkiw, R.: Volume conserving finite element simulations of deformable models. ACM Trans. Graph. **26** (2007)
17. Irving, G., Teran, J., Fedkiw, R.: Invertible finite elements for robust simulation of large deformation. In: Proceedings of the 2004 ACM SIGGRAPH/Eurographics symposium on Computer animation, SCA '04, pp. 131–140. Eurographics Association, Aire-la-Ville, Switzerland, Switzerland (2004)
18. Irving, G., Teran, J., Fedkiw, R.: Tetrahedral and hexahedral invertible finite elements. Graph. Models **68**, 66–89 (2006)
19. Mauch, S.P.: Efficient algorithms for solving static hamilton-jacobi equations. Ph.D. thesis, Pasadena, CA, USA (2003). AAI3093495
20. Muller, M., Dorsey, J., McMillan, L., Jagnow, R., Cutler, B.: Stable real-time deformations. Symposium on Computer Animation: Proceedings of the 2002 ACM SIGGRAPH/Eurographics symposium on Computer animation **21**(22), 49–54 (2002)
21. Müller, M., Gross, M.: Interactive virtual materials. In: Proceedings of Graphics Interface 2004, GI '04, pp. 239–246. Canadian Human-Computer Communications Society, School of Computer Science, University of Waterloo, Waterloo, Ontario, Canada (2004)
22. Müller, M., Heidelberger, B., Hennix, M., Ratcliff, J.: Position based dynamics. J. Vis. Comun. Image Represent. **18**, 109–118 (2007)
23. Müller, M., Heidelberger, B., Teschner, M., Gross, M.: Meshless deformations based on shape matching. ACM Trans. Graph. **24**, 471–478 (2005)
24. Müller, M., Keiser, R., Nealen, A., Pauly, M., Gross, M., Alexa, M.: Point based animation of elastic, plastic and melting objects. In: Proceedings of the 2004 ACM SIGGRAPH/Eurographics symposium on Computer animation, SCA '04, pp. 141–151. Eurographics Association, Aire-la-Ville, Switzerland, Switzerland (2004)

25. O'Brien, J.F., Hodgins, J.K.: Graphical modeling and animation of brittle fracture. In: Proceedings of the 26th annual conference on Computer graphics and interactive techniques, SIGGRAPH '99, pp. 137–146. ACM Press/Addison-Wesley Publishing Co., New York, NY, USA (1999)
26. Ogden, R.: Large Deformation Isotropic Elasticity-On the Correlation of Theory and Experiment for Incompressible Rubberlike Solids. Proceedings of the Royal Society of London. Series A, Mathematical and Physical Sciences (1934-1990) **326**(1567), 565–584 (1972)
27. Pennec, X., Stefanescu, R., Arsigny, V., Fillard, P., Ayache, N.: Riemannian Elasticity: A Statistical Regularization Framework for Non-linear Registration. MICCAI **3750**, 943 (2005)
28. Schmedding, R., Teschner, M.: Inversion handling for stable deformable modeling. Vis. Comput. **24**, 625–633 (2008)
29. Selle, A., Lentine, M., Fedkiw, R.: A mass spring model for hair simulation. ACM Trans. Graph. **27**(3), 1–11 (2008)
30. Si., H.: Tetgen: A quality tetrahedral mesh generator and three-dimensional delaunay triangulator. Opensource Project (2011)
31. Sigg, C., Peikert, R., Gross, M.: Signed distance transform using graphics hardware. In: Proceedings of the 14th IEEE Visualization 2003 (VIS'03), VIS '03, pp. 12–. IEEE Computer Society, Washington, DC, USA (2003)
32. Teran, J., Blemker, S., Hing, V.N.T., Fedkiw, R.: Finite volume methods for the simulation of skeletal muscle. In: Proceedings of the 2003 ACM SIGGRAPH/Eurographics symposium on Computer animation, SCA '03, pp. 68–74. Eurographics Association, Aire-la-Ville, Switzerland, Switzerland (2003)
33. Teran, J., Sifakis, E., Irving, G., Fedkiw, R.: Robust quasistatic finite elements and flesh simulation. In: Proceedings of the 2005 ACM SIGGRAPH/Eurographics symposium on Computer animation, SCA '05, pp. 181–190. ACM, New York, NY, USA (2005)
34. Terzopoulos, D., Platt, J., Barr, A., Fleischer, K.: Elastically deformable models. SIGGRAPH Comput. Graph. **21**, 205–214 (1987)
35. Teschner, M., Heidelberger, B., Muller, M., Gross, M.: A versatile and robust model for geometrically complex deformable solids. In: CGI '04: Proceedings of the Computer Graphics International, pp. 312–319. IEEE Computer Society, Washington, DC, USA (2004)
36. Wicke, M., Ritchie, D., Klingner, B.M., Burke, S., Shewchuk, J.R., O'Brien, J.F.: Dynamic local remeshing for elastoplastic simulation. ACM Trans. Graph. **29**, 49:1–49:11 (2010)
37. Wright, J.N.S.J.: Numerical Optimization, second edition edn. Springer Verlag (2006)
38. Zhu, Y., Sifakis, E., Teran, J., Brandt, A.: An efficient multigrid method for the simulation of high-resolution elastic solids. ACM Trans. Graph. **29**, 16:1–16:18 (2010)